Alterations in physical state of silver nanoparticles exposed to synthetic human stomach fluid.

Kim R Rogers[a]*, Karen Bradham[b], Thabet Tolaymat[c], David J. Thomas[b], Thomas Hartmann[d], Longzhou Ma[d], Alan Williams[a]

[a]*U.S. Environmental Protection Agency, Las Vegas, NV, USA*
[b]*U.S. Environmental Protection Agency, Research Triangle Park, NC, USA*
[c]*U.S. Environmental Protection Agency, Cincinnati, OH, USA*
[d]*University of Nevada, Harry Reid Center for Environmental Studies, Las Vegas, NV, USA*

Abstract

The bioavailability of ingested silver nanoparticles (AgNPs) depends in large part on initial particle size, shape and surface coating, properties which will influence aggregation, solubility and chemical composition during transit of the gastrointestinal tract. Citrate-stabilized AgNPs were exposed to synthetic human stomach fluid (SSF) (pH 1.5) and changes in size, shape, zeta potential, hydrodynamic diameter and chemical composition were determined during a 1 hr exposure period using Surface Plasmon Resonance (SPR), High Resolution Transmission Electron Microscopy/ Energy Dispersive X-ray Spectroscopy (TEM/EDS), Dynamic Light Scattering (DLS) and X-ray Powder Diffraction (XRD) combined with Rietveld analysis. Exposure of AgNPs to SSF produced a rapid decrease in the SPR peak at 414 nm and the appearance of a broad absorbance peak in the near infrared (NIR) spectral region. During exposure to SSF, changes in zeta potential, aggregation and morphology of the particles were also observed as well as production of silver chloride which appeared physically associated with particle aggregates.

Key Words: Silver nanoparticles, Synthetic stomach fluid, Nanoparticle characterization, Exposure, Bioavailability

*Corresponding author at: U.S. Environmental Protection Agency, 944 E. Harmon Ave., Las Vegas, NV 89119. E-mail: rogers.kim@epa.gov

1. Introduction

The anti-microbial activities of silver nanoparticles (AgNPs) have lead to their incorporation into a many consumer products, including fabrics (Blaser et al., 2008), dietary supplements, laundry detergents, body soap, toothbrushes, toothpaste, disinfectant sprays, kitchen utensils, and children's toys (Kim et al., 2010; PEN, 2012). Increased manufacture, marketing, and use of AgNP-containing household and personal care products has prompted concerns about potential for human exposure to both AgNPs and other forms of silver (Wijnhoven et al., 2009). Given the forms,

uses, and potential misuses of consumer products containing AgNPs, ingestion of AgNPs may be a significant route for unintentional exposure. There is a substantial literature on the toxicity of soluble and insoluble silver compounds including colloidal silver preparations which are likely to contain particles smaller than 100 nm (Drake and Hazelwood, 2005; ATSDR, 2005). Based on these data, the U.S. Environmental Protection Agency (U.S. EPA) has suggested that drinking water concentrations of total Ag should not exceed 0.05 mg/L with short term concentrations not to exceed 1.142 mg/L (ATSDR, 2005). It is unclear whether guidelines developed for Ag in other physical forms are sufficient to assess risks associated with exposure to nanoparticulate Ag. Hence, research is underway to assess effects of the unique physical and chemical properties of AgNPs on their absorption, distribution, and toxic effects (U.S. EPA, 2011).

Although systemic absorption of ingested colloidal silver has been examined in humans (White et al., 2003; Chang et al., 2006), neither the physical and chemical characteristics of the silver colloid during transit of the gastrointestinal tract nor the absorbed form of silver (e.g., AgNP, Ag^{+}) is known (Wijnhoven et al, 2009). Studies in other species have provided some information on the fate and effects of ingested AgNPs . Intravenous administration or ingestion of very high doses of colloidal silver in rats results in organ failure and animal death (Schmähl and Steinhoff, 1960). A recent study in rats receiving AgNPs orally for 28 days characterized tissue distribution of Ag and noted evidence of hepatotoxicity (increased serum cholesterol and alkaline phosphatase activity) (Kim et al., 2008). Although such studies are useful, they may not fully account for physiological differences between humans and rodents. For example, of potential relevance to studies of the fate of ingested AgNPs are alterations in particles that occur in the highly acidic environment of the stomach. Notably, the pH of gastric fluid differs markedly between human (pH 1.5) and mouse (pH 3) (Evans et al., 1988; McConnell et al., 2008). This discrepancy suggests that it may be more productive to study particle alterations in an *in vitro* system that more closely resembles the human stomach than does the mouse stomach. This approach may be especially germane as both synthetic methods and mode of surface stabilization affect dependence of surface charge and aggregation behavior of AgNPs on pH and ionic environment (El Badawy et al., 2011). Because bioavailability of ingested AgNPs will likely depend on the aggregation state and chemical properties of particles after modification in the acidic environment of the stomach, the primary objective of this preliminary study was to investigate physical and chemical changes that occur during exposure of AgNPs to synthetic stomach fluid (SSF) system.

2. Methods and Materials

2.1 Materials:

Citrate-stabilized AgNPs (40 nm nominal diameter, Biopure, 1.0 mg/mL) were obtained from Nanocomposix (San Diego, CA). Polyacrylate-stabilized AgNPs with a 1-10 nm nominal diameter range (1.5 mg/mL) were obtained from Vive Nano (Toronto, Canada). Lanthanum hexabromide (LaB_6) that was used as an internal XRD line standard (SRM 660a) was obtained from NIST (Gaithersburg, MD). All other chemicals were reagent grade and obtained from Sigma-Aldrich (St. Louis, MO). Synthetic stomach fluid (SSF) was prepared using deionized distilled (DDI) water and contained HCl (0.42 M) and glycine (0.40 M) pH 1.5 (Kelly et al., 2002).

2.2 Particle exposures:

AgNPs were diluted from stock suspensions as received from the manufacturer to 50 μg/mL for the TEM experiments or used undiluted for XRD experiments. These suspensions were then added (1:1) to the SSF and incubated for 1 hr before centrifugation (3000 x g) for 5 min. Supernates were removed and resulting pellets were re-suspended in DDI water (using brief (5 min) sonication) to their original volume for TEM experiments or to 1/10 of their original volume for XRD experiments.

2.3 TEM and XRD conditions

For TEM, AgNPs were either applied to copper grids coated with Formvar™ membranes or immobilized to amine-functionalized silicon TEM windows (Dune Scientific, Eugene OR) by exposure for 1 min followed by immersion in DDI water for 15 s. Images were acquired at 300 kV using a FEI Tecnai F30 G2 TEM (Hillsboro, OR) with a (2k x 2k pixels) ORIUS SC200D CCD camera, manufactured by Gatan Inc. (Pleasanton, CA). The imaged structures were analyzed by energy dispersive X-ray spectroscopy for elemental composition using an EDAX detector. XRD patterns were obtained using a Bruker-AXS D8 Advance Vario diffractometer (Madison, WI) with a Johansson-type monochromator (λ=1.54063Å at 40 KV, 40 mA). XRD patterns were collected in reflection mode at 25° C and diffracted intensities were fitted using Rietveld analysis applying pseudo-Voigt peak-profile parameters. Structure parameters were refined based on National Institute of Standards and Technology-Inorganic Crystal Structure Database (NIST-ICSD) data.

2.4 Plasmon resonance ultraviolet (UV)-visible spectroscopy, zeta potential and hydrodynamic diameter

UV-visible spectra were collected using a Hewlett Packard single beam instrument (Agilent, Santa Clara, CA) at 25°C. Concentrated AgNP suspensions were diluted with DDI water to an initial absorbance of 1.0 then diluted (1:1) in SSF. Spectra were recorded in the second to minute timeframe. The hydrodynamic diameter (HDD) and zeta potential of the AgNP were measured using a Zetasizer Nanoseries (Malvern Instruments, Southbourough, MA). Measurements were taken after dilution of the 40 nm AgNP (as provided by the manufacturer) 1:10 in either SSF or DDI.

3. Results

Citrate-stabilized AgNPs (nominal diameter of 40 nm) suspended in DDI water showed a plasmon resonance peak at 414 nm. The absorbance spectrum was stable during a 1 hr exposure to DDI water. However, when particles were diluted in SSF, the peak absorbance at 414 nm rapidly declined and a broad red shifted peak was observed at around 820 nm (Fig. 1). Decline of the 414 nm peak initially corresponded with increased absorption around 820 nm. Absorbance in 820 nm range began to slightly decrease after 2 min exposure to SSF (Fig. 2). AgNPs with a smaller and more variable size distribution (1-10 nm nominal diameters) obtained from a second vendor exhibited a similar pattern of absorbance change upon exposure to SSF (Figs. S1, S2). As measured by DLS, the average HDD of the 40 nm AgNPs significantly increased from 40 nm to 300 nm over a 30 min period when exposed to SSF (Fig. 3) The HDD of the AgNPs did not change when diluted into DDI. In addition, the zeta potential decreased from -34 mV in DDI to approximately -4 mV in SSF.

FIGURES 1, 2 & 3

TEM observation of nominal 40 nm particles before exposure to SSF showed small clusters of spherical particles with distinct perimeters consistent with a mondisperse suspension (Fig 4a). The EDS spectrum showing the presence of Ag, Si, and O was consistent with AgNPs bound to the SiO_2 substrate grid (Fig 4b). Figure 4c shows a TEM image of AgNPs that were exposed to SSF for 10 s before immobilization on the TEM substrate. In contrast to the untreated control

particles, even a brief exposure to SSF produced particles that appeared to be sintered with a lower contrast material forming among particles. Notably, addition of SSF to the AgNP (nominal 40 nm) suspension immediately changed the color of the suspension from yellow to gray (Fig. S3). A similar change in appearance (from brown to tan) upon addition of SSF was also noted with smaller particles (1-10 nm) (Fig.S4). Changes in localized surface plasmon resonance spectra of the AgNPs (which contribute to their observed color)have been shown to be sensitive to both particle size, due to coupling, as well as changes in their dielectric environment from surface bound molecules (Malinsky et al., 2001).

After a 1 hr exposure to SSF, TEM images showed AgNPs to be morphologically distinct from the AgNPs not exposed to SSF. Exposed particles were aggregated and fused with fewer distinct boundaries defining individual particles (Fig. 4d). The EDS spectrum for 40nm AgNPs exposed to SSF for 1 hr showed the additional presence of chloride (Fig. 4e). The observed change in morphology of the AgNP-aggregates was likely due to the formation of AgCl at the particle surface. In support of this concept, when Ag^+ in the form of $AgNO_3$ solution was added to SSF the immediate formation of a slightly off-white precipitate was noted indicative of the presence of insoluble AgCl (Fig. 4f). TEM observation of the AgCl formed from Ag^+ treated with SSF showed large (>10 μm) aggregates consisting of many particles and smaller aggregates consisting of fewer particles. AgCl particles present in smaller aggregates were 1-2 μm with smaller (50 nm) particles bound to the surface. EDS analysis of aggregated AgCl showed that both Ag and Cl were present (Fig. 4g).

FIGURE 4

X-ray diffraction patterns were obtained for three types of samples. Samples included (Fig. 5a) AgCl precipitated from soluble Ag^+ exposed to SSF, (Fig. 5b) AgNPs that were exposed to SSF for 1 hr and (Fig. 5c) untreated AgNP. Addition of a solution of $AgNO_3$ to SSF (1:1) resulted in the immediate formation of an off-white precipitate identified as AgCl by XRD (Fig. 5a). The most prominent diffraction peaks for the (111), (002), (022), (311) and (222) planes of AgCl were positioned at 27.8°, 32.2°, 46.2°, 54.8° and 57.5° on the 2θ axis (features indicated under the - •- symbol). Features for the LaB_6 standard added to the sample are indicated by the (⊕) symbol. AgNPs exposed to SSF were also analyzed by XRD. After 1 hr incubation of the 40 nm AgNP in SSF, diffraction signal features for both metallic silver and those for AgCl (chlorargyrite) were observed (Fig. 5b). The additional diffraction peaks centered at 2θ = 38.2°, 44.4°, 64.5°and 77.5°

matched the (111), (002), (004) and (311) lattice planes of metallic Ag (features indicated by ∇). Figure 5c shows the diffraction pattern for the 40 nm control AgNPs. The metallic AgNPs showed a cubic structure with features again identified by the∇ symbols and peak widths were suggestive of small (12 nm) crystallites. Although relatively small, the diffraction pattern showed features for metallic silver in addition to the LaB_6 standard.

One of the questions addressed using these in vitro simulation experiments involved the differences between exposure of nanoscale silver particles and bulk silver (as represented by micron-scale particles) to SSF. Table 1 shows the relative amounts of AgCl formed by exposure of different forms of silver to SSF. $AgNO_3$ was fully converted to AgCl after a ten min exposure to SSF. Both 40 nm AgNPs and smaller (1-10 nm) AgNPs showed intermediate levels of AgCl formation after 1 hr exposure to SSF. The surface area for the AgNP (for a given mass) was significantly higher for both of the AgNP preparations than for the micron-scale particles. Exposure of bulk metallic silver (1.6-2.6 μm) did not result in the formation of AgCl in a 1 hr timeframe.

Equilibrium speciation calculations were performed using MINEQL+ ver. 4.62 (Schecher and McAvoy, 2003) to model exposure of the 40 nm AgNP after exposure to the HCl concentration in the SSF. Components used in the calculations included H^+, Ag^+ and Cl^- at pH 1.5. An initial silver ion concentration of 55 μM was estimated using XRD data (with the preliminary assumption that most of the Ag^+ released would be converted to AgCl) (Table 1). Under acidic conditions, calculations suggested the following percentage silver species: precipitated AgCl, 81.1%; $AgCl_2^-$, 13.8%; $AgCl_3^{2-}$, 3.0%; $AgCl_4^{3-}$, 1.4% and soluble AgCl, 0.7%.

4. Discussion

Silver nanoparticles show a unique optical absorbance spectrum that depends on their size, shape, coating agent and interaction between the particles and the components of the matrix in which they are suspended (Dadosh, 2009). The 40 nm citrate-stabilized AgNPs examined in the present study exhibited a spectrum with a characteristic absorption peak at 414 nm. This peak was similar in shape and wavelength maximum to the UV-visible spectrum reported by the manufacturer (www.nanoComposix.com) and similar to a absorbance peak detected in spectra of AgNPs in the same size range from several commercial sources (MacCuspie et al., 2011). Upon addition of SSF, we observed that the AgNP suspension became visibly lighter and cloudy. A similar observation as has been reported to occur after addition of nitric

acid to uncoated AgNPs (Elzey and Grassian, 2010). These authors also observed a significant change in zeta potential from -42.7 mV to near zero mV and reduced stability of the suspension when pH was reduced from neutrality to 1.5.

Again, we similarly observed a significant reduction in zeta potential for the 40 nm citrate-stabilized AgNPs when exposed to SSF. Although similar changes in agglomeration and zeta potential were observed as a function of low pH values, in these cases it is important to note that these variables depend, to a significant extent, on the particle size distribution and surface modification applied to silver nanoparticles (El Badawy et al., 2010). These authors also observed significant differences in ionic strength-induced and pH-induced aggregation in AgNPs with different coatings suggesting that surface modification must be considered when describing the aggregation behavior of AgNPs.

The appearance of an absorbance peak in the near infrared region of the spectrum of AgNPs after addition of strongly acidic SSF may be a consequence of particle interactions that were observed by TEM (see Fig. 4d). A similar broad absorbance peak in the NIR has been attributed to strong coupling between AgNPs due to aggregation (Deivaraj et al, 2005). This spectral evidence of particle-particle interactions is consistent with the sintered appearance of SSF-exposed AgNPs in TEM micrographs (see Fig. 4d). In addition to morphological changes in SSF-exposed AgNPs, the presence of particle-bound Cl in the EDS spectrum of SSF-treated AgNPs suggests that AgCl is formed on particles in this highly acidic environment. Equilibrium speciation calculations further suggest that the released Ag^{+} would predominantly precipitate as AgCl (81.1%). A similar transformation of Ag into AgCl has been reported (Sun, 2010). For that experiment, Ag nanowires were converted into AgCl nanowires by reduction of Fe^{3+} and oxidation of Ag^{0} in the presence of Cl^{-}. It has been further suggested by Impellitteri et al. (2009) and Scheckel et al. (2010), that in the presence of an oxidizer and Cl^{-}, a significant portion of AgNP will be converted to AgCl precipitate which may form a coating on the particle surface. Oxidation of AgNPs and formation of AgCl in SSF observed in the current study are also consistent with the results that, in an oxidizing environment, AgNPs can participate in cooperative oxidation involving protons and dissolved oxygen resulting in the release of Ag^{+}(Liu and Hurt, 2010). Another study indicated that small (8 nm) AgNPs dissolved in the presence of HCl to form insoluble AgCl (Li and Zhu, 2006).

Both the TEM/EDS data showing the presence of Cl associated with SSF-exposed AgNPs and the XRD data show significant conversion of AgNPs to AgCl (see Table 1, Fig. 5b). The extent of conversion to AgCl is influenced by particle

size. Over a 1 hr period of SSF exposure, smaller AgNPs (1-10 nm) show the highest fractional conversion and the bulk silver particles (> 1μm) are not converted to AgCl. Particle size is known to affect formation of AgCl from silver. Although AgNP were converted to AgCl over a three-day exposure to HCl, metallic Ag powder (200 mesh ~ 74 μm) was not converted to AgCl (Li and Zhu, 2006). Surface area-based release kinetics can be used to rationalize differences in apparent rates of oxidative silver dissolution between bulk silver and nanoparticulate forms (Liu & Hurt, 2010). For example, these authors observed 5 orders of magnitude difference in the release rates of ionic Ag from AgNPs and bulk Ag foil that was explained as function of surface area.

In summary, the results reported here indicate a multistep process occurs after the exposure of AgNPs to SSF. First, AgNPs rapidly aggregate possibly due to a change in zeta potential that occurs in acidic media. Second, Ag ions are released from particles by oxidation in acidic media. Third, in the presence of Cl^-, AgCl is formed in proximity to particles and appears to sinter particles together. These reactions can be summarized as

$$2Ag_{(s)} + \tfrac{1}{2}O_2 + H^+ \longrightarrow 2Ag^+ + H_2O$$

$$2Ag^+ + 2Cl^- \longrightarrow 2AgCl$$

$$2Ag_{(s)} + \tfrac{1}{2}O_2 + 2H^+ + 2Cl^- \longrightarrow 2AgCl + H_2O$$

In the current study, AgNPs were exposed to SSF for 1 hr; however, the interval for exposure of ingested AgNPs to the acidic environment of the human stomach may vary considerably among individuals. Thus, the extent of solubilization of Ag from nanoparticles and its conversion to AgCl may vary as a function of residence time in the stomach. The presence of metal or metal ion coordinating moieties (e.g., sulfhyryl, carboxylate and amine groups) present in food may also influence the dissolution and precipitation of Ag from AgNP. Additional studies of the formation and fate of Ag species in the stomach following AgNP ingestion will be needed to clarify these issues. Similarly, studies of changes in physical and chemical states of AgNP that occur in distal portions of the gastrointestinal

tract after residency in the stomach should be examined to develop a comprehensive picture of the factors affecting bioavailability of metals from ingested nanoparticles.

5. Conclusion

In humans, bioavailability of ingested AgNPs will likely depend on a number of factors including particle size distribution, shape, chemical coating, and transformation processes that occur during transit of the gastrointestinal tract. The present study with a simple *in vitro* model of the human stomach shows that citrate-stabilized AgNPs agglomerate and partially react to form AgCl during exposure to SSF. Aggregation of AgNPs seen in this study may influence the production of AgCl. Hence, ingested AgNPs may be converted to a variety of aggregated and chemically modified particles in the stomach. It is noted that these data describe a preliminary investigation of AgNPs stabilized by either citrate or polyacrylate. Given the wide range of coating compounds that vary in chemical properties, surface charge, etc., the herein reported results may not be representative of AgNP preparations in general. Bioavailability of Ag from these Ag-containing materials will also depend on the interactions between this mixture of Ag-containing species and the absorptive surfaces of the gastrointestinal tract. Disclaimer: The United States Environmental Protection Agency (EPA), through its Office of Research and Development (ORD), has funded and managed the research described here. It has been subjected to the Agency's administrative review and has been approved for publication. Mention of trade names or commercial products does not constitute endorsement or recommendation for use. Acknowledgements: The authors would like to thank Gerald Egeland for his technical contribution to the XRD analysis.

6. References

Agency for Toxic Substance and Disease Registry (ATSDR). Toxprofiles 2005. Atlanta, GA; Department of Health and Human Services.

Blaser SA, Scheringer, M, MacLeod M, Hungerbuhler K. Estimation of cumulative aquatic exposure and risk due to silver: Contribution of nano-functionalized plastics and textiles. Sci Total Environ 2008; 390:396-409.

Chang ALS, Khosravi V, Egbert B. A case of argyria after colloidal silver ingestion. JCutan Pathol 2006; 33: 809-11.

Dadosh T. Synthesis of uniform silver nanoparticles with a controllable size. Mater Lett 2009; 63: 2236-8.

Deivaraj TC, Lala NL, Lee JY. Solvent-induced shape evolution of PVP protected spherical silver nanoparticles into triangular nanoplates and nanorods. J Colloid Interface Sci 2005**;** 289**:** 402-9.

Drake PL, Hazelwood KJ. Exposure-related health effects of silver and silver compounds: A review. Ann Occupational Hygiene 2005; 49: 575-85.

El Badawy A M, Luxton TP, Silva RG, Scheckel KG, Suidan MT, Tolaymat TM. Impact of Environmental Conditions (pH, Ionic Strength, and Electrolyte Type) on the Surface Charge and Aggregation of Silver Nanoparticles Suspensions." Environ Sci Technol 2010; 44: 1260-66.

El Badawy A M, Silva RG, Morris B, Scheckel KG, Suidan MT, Tolaymat TM. Surface charge-dependent toxicity of silver nanoparticles. Environ Sci Technol 2011; 45: 283-7.

Elzey S, Grassian VH. Agglomeration, isolation and dissolution of commercially manufactured silver nanoparticles in aqueous environments. J Nanopart Res 2010; 12: 1945-58.

Evans DF, Pye G, Bramley R, Clark AG, Dyson TJ, Hardcastle JD. Measurement of gastrointestinal pH profiles in normal ambulant human subjects. Gut 1988; 29: 1035-41.

Impellitteri CA, Tolaymat TM, Scheckel KG. The speciation of silver nanoparticles in antimicrobial fabric before and after exposure to hypochlorite/detergent solution. J Environ Qual 2009; 38: 1528-30.

Kelly ME, Brauning SE, Schoof RA, Ruby MV. Assessing Oral Bioavailability of Metals in Soil. Columbus:Battelle Press, 2002.

Kim YS, Kim JS, Cho HS, Rha SD, Kim JM, Park JD, et al. Twenty-eight-day oral toxicity, genotoxicity, and gender-related tissue distribution of silver nanoparticles in Sprague-Dawley rats. Inhalation Toxicol 2008; 20: 575-83.

Kim YS, Song MY, Park JD, Song KS, Ryu HR, Chung YH, et al. Subchronic oral toxicity of silver nanoparticles. Particle Fibre Toxicol 2010; 7: 20-2.

Li L, Zhu YJ. High chemical reactivity of silver nanoparticles toward hydrochloric acid. J Colloid Interface Sci 2006; 303: 415-18.

Liu JY, Hurt RH. Ion Release Kinetics and Particle Persistence in Aqueous Nano-Silver Colloids. Environ Sci Technol 2010; 44: 2169-75.

Liu JY, Sonshine DA, Shervani S, Hurt RH. Controlled Release of Biologically Active Silver from Nanosilver Surfaces. ACS Nano 2010; 4: 6903-13.

MacCuspie RI, Rogers KR, Patra M, Suo ZY, Allen AJ, Martin MA, et al. Challenges for physical characterization of silver nanoparticles under pristine and environmentally relevant conditions. J Environ Monit 2011; 13: 1212-26.

McConnell EL, Basit AW, Murdan S. Measurements of rat and mouse gastrointestinal pH, fluid and lymphoid tissue, and implications for in-vivo experiments. J Pharm Pharmacol 2008; 60: 63-70.

Schecher WD, McAvoy DC. MINEQL+ A software environment for chemical equilibrium modelong. Computers Environ Urban Syst 1992; 16: 65-76.

Scheckel KG, Luxton TP, El Badawy AA, Impellitteri CA, Tolaymat TM. Synchrotron speciation of silver and zinc oxide nanoparticles aged in a kaolin suspension. Environ Sci Technol 2010; 44, 1307-12.

Schmähl D, Steinhoff D. Versuche zur Krebserzeugung mit kolloidalen Silber-und Goldlosungen an Ratten [Experimental carcinogenesis in rats with colloidal silver and gold solutions] Z Krebsforsch 1960; 63: 586-91.

Sun YG. Conversion of Ag Nanowires to AgCl Nanowires Decorated with Au Nanoparticles and Their Photocatalytic Activity. Journal of Physical Chemistry C 2010; 114: 2127-33.

Project on Emerging Nanotechnologies (PEN) (www.nanoproject.org/inventories/consumer/browse/products). Accessed January, 2012.

U.S. Environmental Protection Agency. Nanotechnology Research (accessed 2011). (www.epa.gov/nanoscience/).

White JML, Powell AM, Brady K, Russell-Jones R. Severe generalized argyria secondary to ingestion of colloidal silver protein." Clin Experiment Dermatol 2003; 28: 254-56.

Wijnhoven SWP, Peijnenburg WJGM, Herberts CA, Hagens WI, Oomen AG, Heugenss EHW, et al. Nano-silver - a review of available data and knowledge gaps in human and environmental risk assessment. Nanotoxicology 2009; 3: 109-78.

Table 1
Effect of particle size on the conversion of Ag to AgCl during exposure to human synthetic stomach fluid (XRD/Rietveld).

Particle size	SSF incubation time (min)	Calculated wt.%	
		Ag	AgCl
Bulk Ag	0	100	0
Bulk Ag	60	100	0
AgNP (40 nm)	0	100	0
AgNP (40 nm)	60	76	24
AgNP (1-10 nm)	0	100	0
AgNP (1-10 nm)	60	69	31
$AgNO_3$ (soln)	10	0	100

Fig. 1. Absorbance spectra for AgNP (40 nm, citrate-stabilized) exposed to SSF for specified times. Plasmon resonance peaks were at 414 nm and 820 nm.

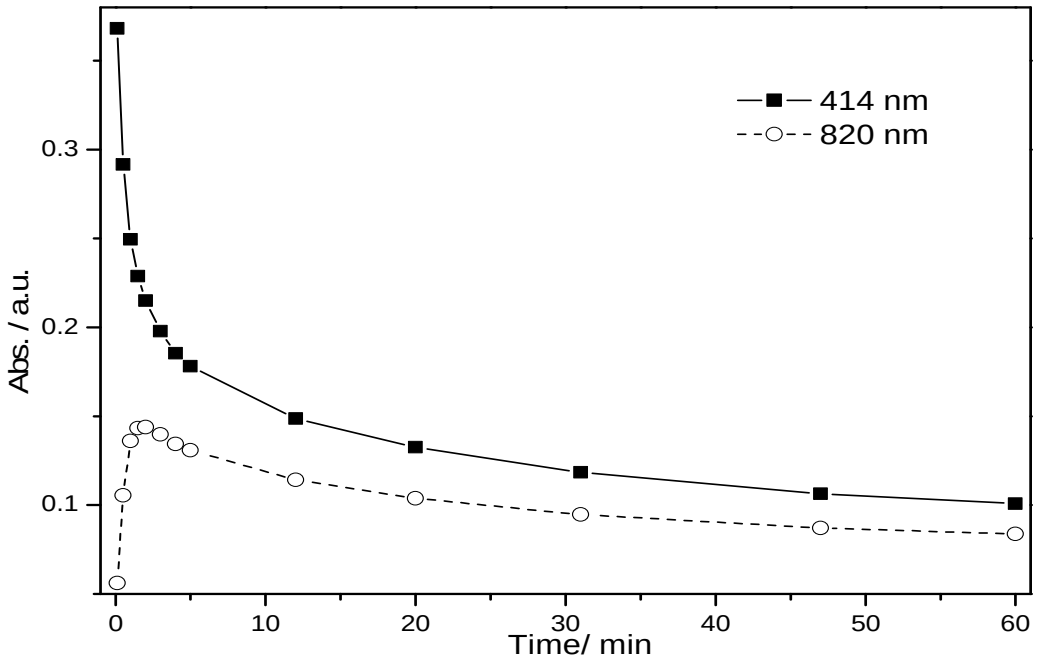

Fig. 2 Change in absorbance for AgNP (40 nm, citrate-stabilized) at 414 nm and 820 nm over a 60 min exposure to SSF.

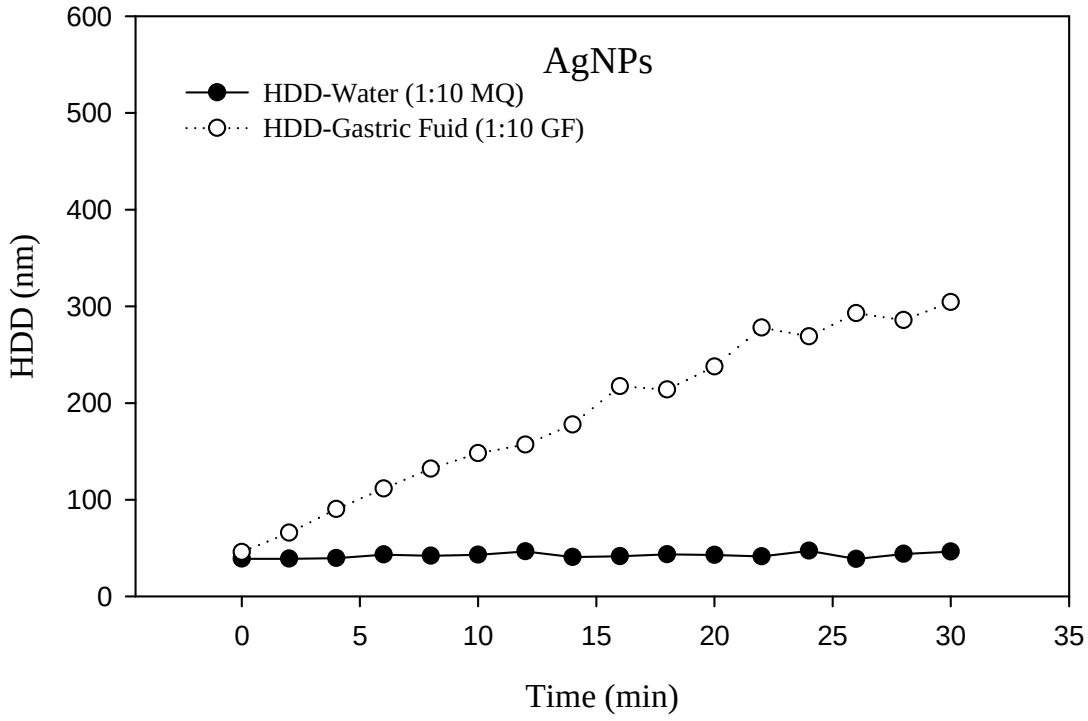

Fig. 3 Hydrodynamic diameter of AgNP (40 nm, citrate-stabilized) exposed to gastric fluid (GF), identical to SSF, or MQ, identical to DDI water, measured by dynamic light scattering.

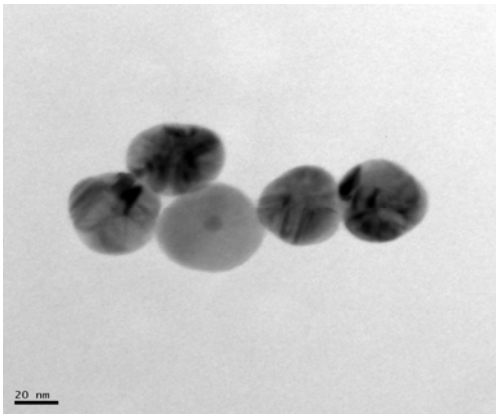
20 nm

(a)

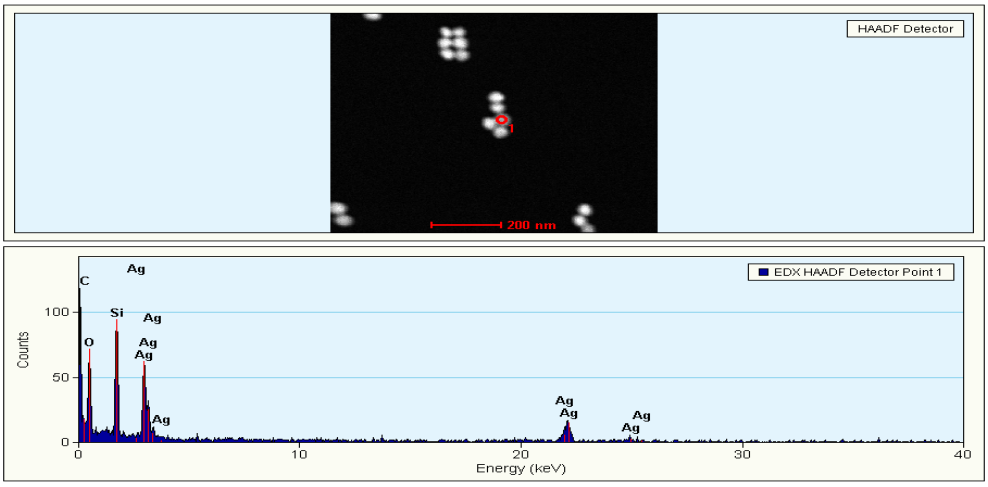
HAADF Detector
200 nm
EDX HAADF Detector Point 1
Counts
Energy (keV)
C
O
Si
Ag

(b)

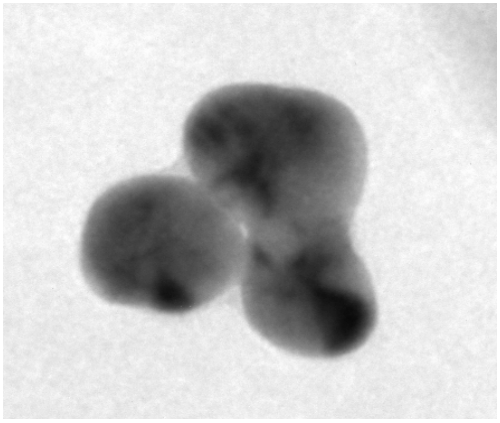

(c)

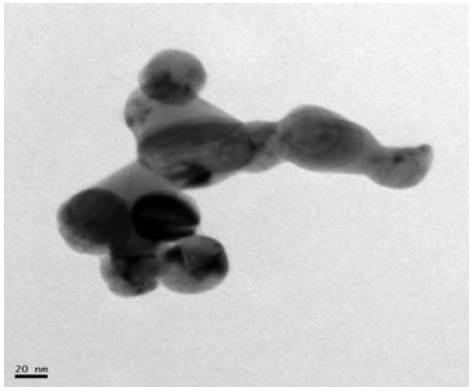
20 nm

(d)

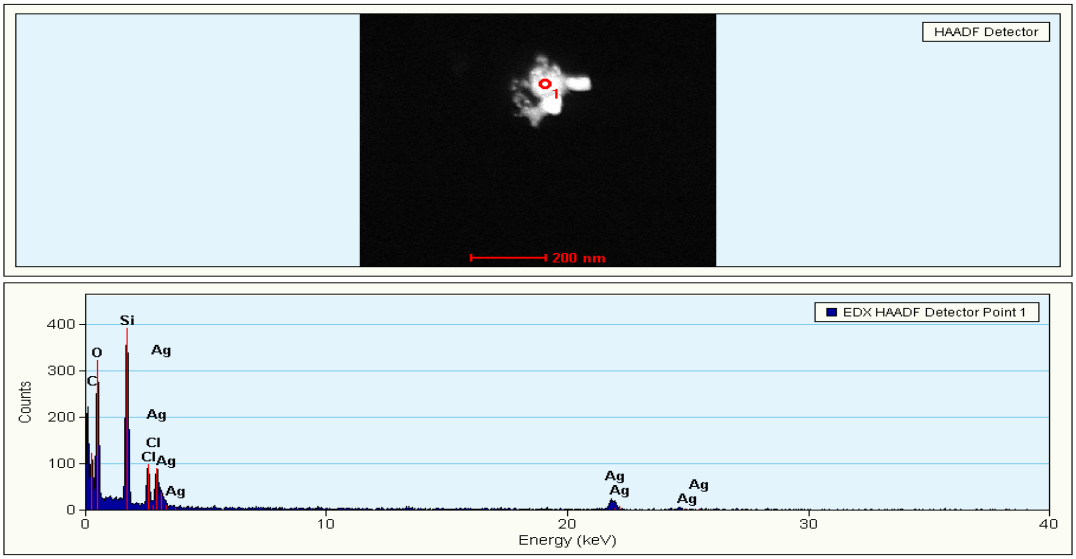
HAADF Detector
1
200 nm
EDX HAADF Detector Point 1
Si
O
C
Ag
Ag
Cl
Cl
Ag
Ag
Ag
Ag
Ag
Ag
Counts
Energy (keV)
0
100
200
300
400
0
10
20
30
40

(e)

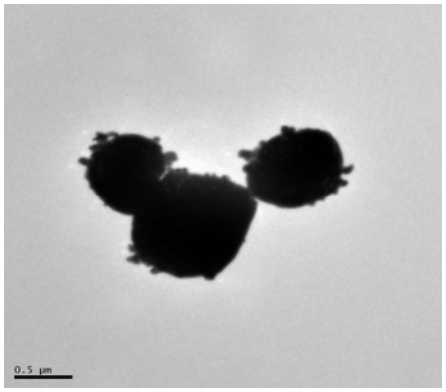
0.5 µm

(f)

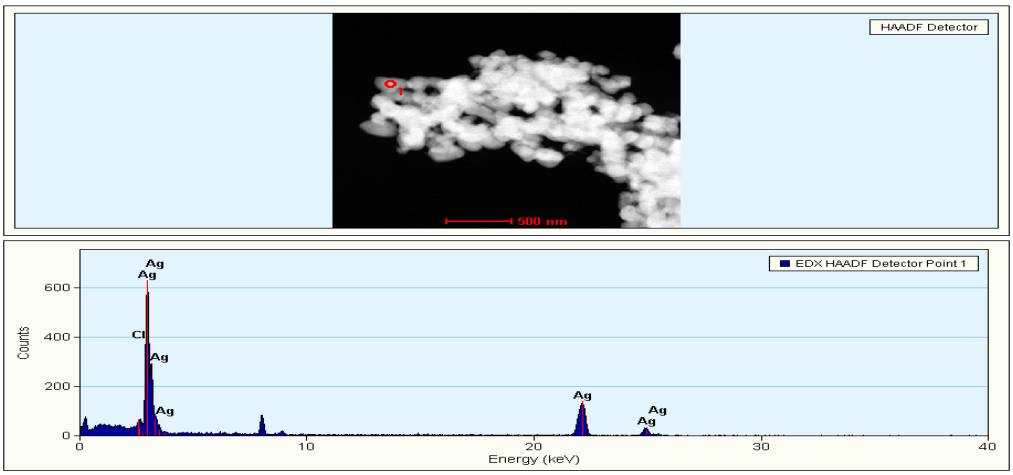

(g)

Figure 4 (a) TEM micrograph of unexposed (control) AgNP (40 nm). Particles were immobilized to amine-modified SiO_2 TEM grids, (b) TEM micrograph and EDS spectrum of unexposed (control) AgNP (40 nm). Particles were immobilized to amine-modified SiO_2 TEM grids, (c) TEM micrograph of AgNP (40 nm) exposed to SSF for 10s. Particles were immobilized to amine-modified SiO_2 TEM grids, (d) TEM micrograph of AgNP (40 nm) exposed to SSF for 1 hr. Particles were immobilized to amine-modified SiO_2 TEM grids (e) TEM micrograph and EDS spectrum of AgNP (40 nm) after 1 hr exposure to SSF. Particles were immobilized to amine-modified SiO_2 TEM grids, (f) TEM micrograph for particles formed from silver nitrate and SSF (10 min), (g) TEM micrograph and EDS spectrum for particles formed from silver nitrate and SSF (10 min).

Figure 5. XRD patterns and Rietveld analysis for (a) precipitate resulting from silver nitrate and SSF (10 min); (b) silver nanoparticles (40 nm) exposed to SSF for 1 hr; and (c) untreated silver nanoparticles, 40 nm.